Supporting Information

Photophysical Dynamics of the Efficient Emission and Photosensitization of $[Ir(pqi)_2(NN)]^+$ Complexes

Kassio P.S. Zanoni, Akitaka Ito, Malte Grüner, Neyde Y. Murakami Iha and Andrea S. S. de Camargo

General Experimental Procedures

Measurements for structural characterization

^{1}H NMR spectra were recorded using a Bruker AIII 500 (500 MHz) or an INOVA 300 (300 MHz) spectrometer, using CD3CN as solvent. The residual solvent signals were employed as internal standards.

Mass spectroscopy was performed using a Bruker Daltonics MAXIS HD.

Photophysical measurements

UV-Vis absorption spectra were recorded on a Hewlett-Packard diode array spectrophotometer model 8453. Steady-state and time-resolved emission spectra were recorded using a Horiba Fluorolog time-correlated single photon-counting or an ISS-PC1 photon-counting spectrofluorometer. For experiments using the Horiba Fluorolog, a xenon lamp (λ_{exc} = 365 nm, 1 nm bandwidth, 400 nm long pass filter) or a Horiba Delta Diode source (λ_{exc} = 370 nm, frequency = 20 kHz) were employed as excitation sources for steady-state or time-resolved measurements, respectively. When using the ISS-PC1, a xenon lamp (λ_{exc} = 365 nm, 2 nm bandwidth, 389 nm long pass filter) or an ISS laser (λ_{exc} = 378 nm, frequency = 20 kHz) were employed. Emission intensities (photon counting) of steady-state spectra were corrected for the system spectral response. For room temperature measurements, the absorbance of sample solutions in acetonitrile was set between 0.1 and 0.3 in a quartz cuvette with 1.000 cm optical path length. Solutions were

deoxygenated with N_2 or Ar for at least 10 minutes prior to measurement. For 77 K experiments, samples were prepared in a 4/5 (v/v) mixture of propionitrile/butyronitrile (prop:but) in cylindrical quartz tubes, 0.4 cm radius, and were inserted into a Dewar flask containing liquid N_2.

Absolute emission quantum yields (ϕ_0) of the complexes in degassed acetonitrile at room temperature were measured applying the methodology described by de Mello *et al.*,[1] using a $BaSO_4$ coated integrating sphere, Horiba Quanta-ϕ, with samples positioned in its center.

The radiative (k_r) and nonradiative decay (k_{nr}) rates were calculated by Equations SI1a and SI1b,

$$k_r = \frac{\phi_0}{\tau_0} \qquad (SI1a)$$

$$k_{nr} = \frac{1 - \phi_0}{\tau_0} \qquad (SI1b)$$

in which τ_0 is the emission lifetime of the sample in degassed solvent.

Singlet oxygen quantum yields (Φ_Δ) in deuterated acetonitrile were obtained from Equation SI2 [2,3] using $[Ru(bpy)_3]^{2+}$ in the same solvent as a reference ($\Phi_\Delta = 0.57$ [4]),

$$\Phi_\Delta^s = \Phi_\Delta^{Ref} \frac{I^s}{I^{Ref}} \frac{1 - 10^{-A^{Ref}}}{1 - 10^{-A^s}} \qquad (SI2)$$

in which Φ_Δ^s is the singlet oxygen quantum yield of the sample, Φ_Δ^{ref} is the singlet oxygen quantum yield of the reference, A^s and A^{ref} are the absorbances at the excitation wavelength of sample and reference solutions; I^s and I^{ref} are the integrals of the oxygen's emission spectrum for sample and reference solutions.

The quenching rate constant (k_q) was obtained by Stern–Volmer analyses using Equation SI3,[5]

$$\frac{\phi_0}{\phi} = k_q \tau_0 [^3O_2] + 1 \qquad (SI3)$$

in which ϕ is the emission quantum yield of the complex in a sample solution with a known [$^3O_2$] concentration and τ_0 is the T_1's lifetime in the degassed solution.

The *x* and *y* CIE coordinates were calculated by Equations SI4a and SI4b from their *X*, *Y* and *Z* tristimulus, Equations SI5a to SI5c, using photoluminescence spectral data in acetonitrile at 298 K. The numerical values of the CIE standard $\bar{x}(\lambda)$, $\bar{y}(\lambda)$ and $\bar{z}(\lambda)$, are available as online free-access tables.[6]

$$x = \frac{X}{X + Y + Z} \qquad (SI4a)$$

$$y = \frac{Y}{X + Y + Z} \qquad (SI4b)$$

$$X = \int_{380}^{780} I(\lambda)\bar{x}(\lambda)d\lambda \qquad (SI5a)$$

$$Y = \int_{380}^{780} I(\lambda)\bar{y}(\lambda)d\lambda \qquad (SI5b)$$

$$Z = \int_{380}^{780} I(\lambda)\bar{z}(\lambda)d\lambda \qquad (SI5c)$$

Franck-Condon spectral analyses

In the fitting procedure, E_0, $\hbar\omega$, *S* and $\tilde{\nu}_{1/2}$ (Equation 1 in the Article) were optimized with a least-squares minimization routine with application of a Generalized Reduced Gradient (GRG2) algorithm.[7] Prior to the spectral fitting analysis, the number of photons at a given wavelength were corrected to the wavenumber scale by using the relationship,[8] $I(\tilde{\nu}) = I(\lambda) \times \lambda^2$. The summation was carried out from $v^* = 0$ in the excited state to levels $v = 0 \rightarrow 10$ in the ground state.

Theoretical calculations

Molecular-orbital calculations for the complex were conducted with the Gaussian 09W software.[9] Optimization of the ground-state geometry was performed by using DFT with the B3LYP functional. The LanL2DZ[10–12] and 6-31G(d,p)[13,14] basis sets were used to treat iridium and all other atoms, respectively. TD-DFT calculations were then performed to estimate energies and oscillator strengths of the lowest-lying 50 singlet and 3 triplet transitions; the triplet calculations were performed using the singlet-optimized geometries. All the calculations were carried out in acetonitrile as solvent by using a Polarizable Continuum Model (PCM).[15,16] Kohn–Sham orbitals were plotted using GaussView 5.0.[17]

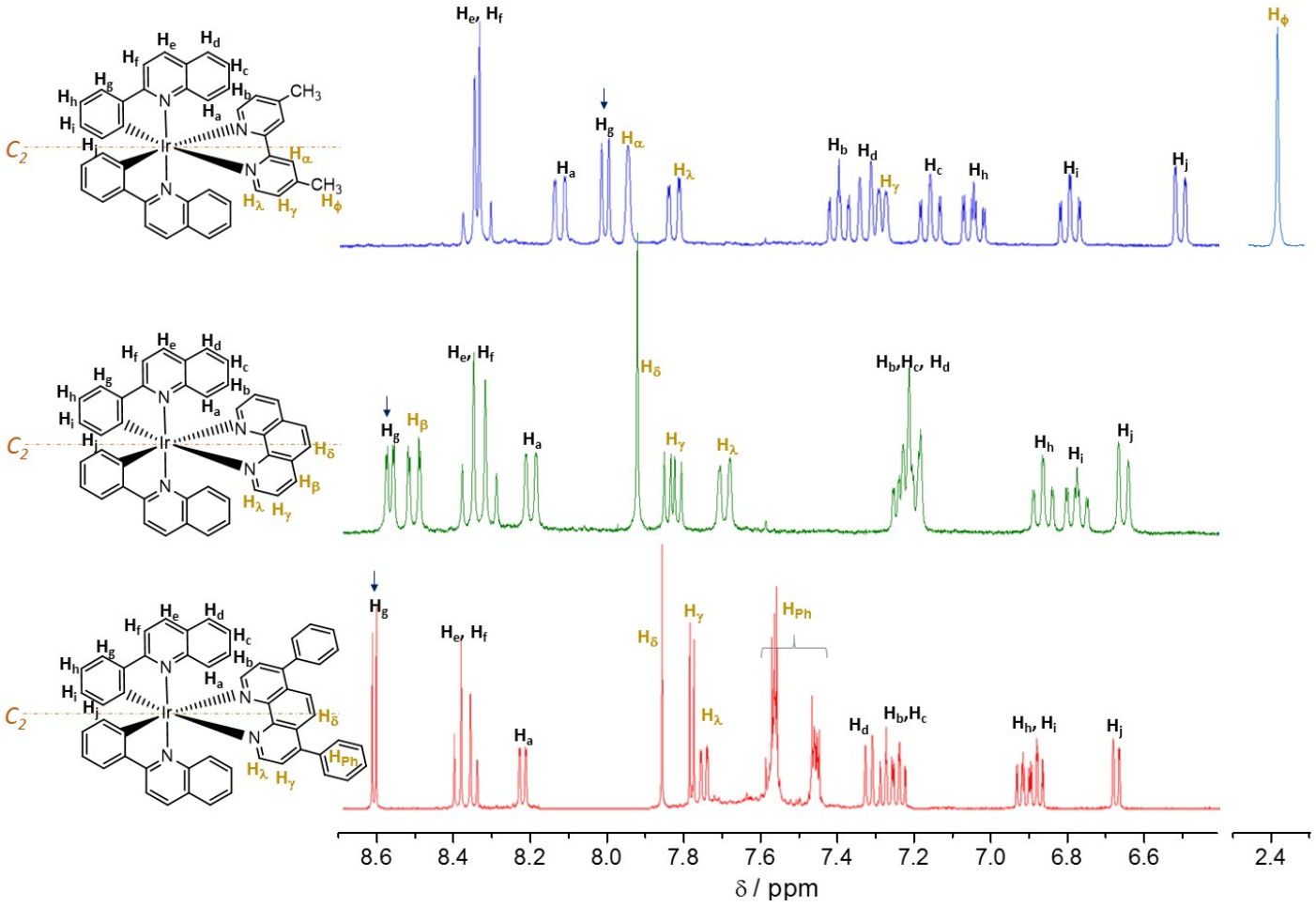

Figure SI1. ^{1}H NMR spectra for the investigated [Ir(*pqi*)$_2$(*NN*)]$^+$ complexes in CD_3CN. For all compounds, the ^{1}H NMR spectra exhibit only one set of ten aromatic signals for *pqi* and one set for the *NN* diimine ligands whose total signal integration is equal to half of the amount of protons in these ligands. These facts indicate the two *pqi* ligands are equivalent and the complex symmetry is C_2, where the C_2 axis bisects the *NN* ligand. Interestingly, the change of the ancillary *NN* ligand leads to electronic perturbations in the phenyl portion of the cyclometalated *pqi* ligand, which holds the organometallic C–Ir bond. The H_g proton (meta to the C–Ir bond), for example, is deshielded by changing the diimine ligand from *dmb* (8.00 ppm) to *phen* (8.57 ppm) then to *Ph$_2$phen* (8.62 ppm) as an evidence to the stronger electron-withdrawing nature of the phenanthroline ligands, as opposed to the electron donation from *dmb*. This effect has interesting consequences on the photophysical characteristics of the complexes, as discussed in the Article. The ^{1}H NMR spectra also indicate that the isolated powders of the synthesized compounds have no impurities.

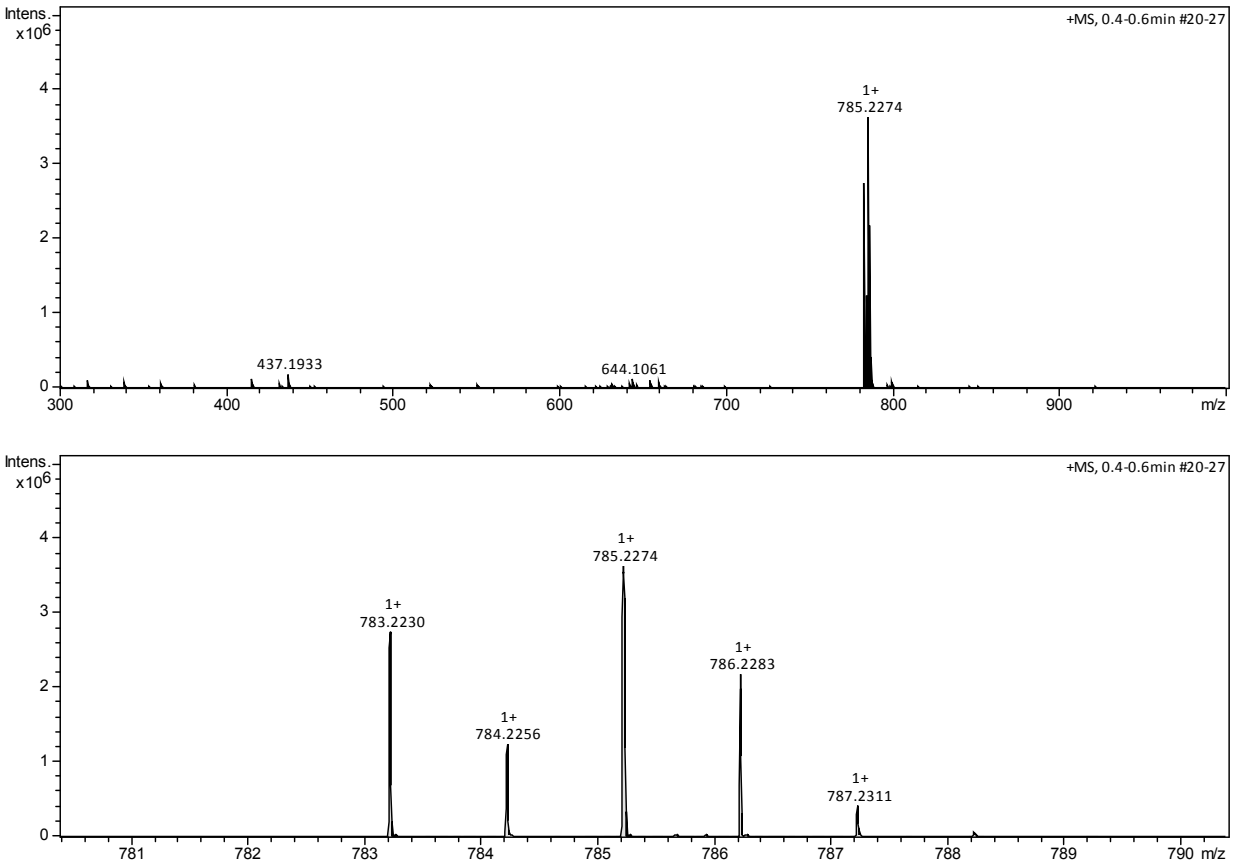

Figure SI2. Mass spectra for **pqiIrDmb** in acetonitrile.

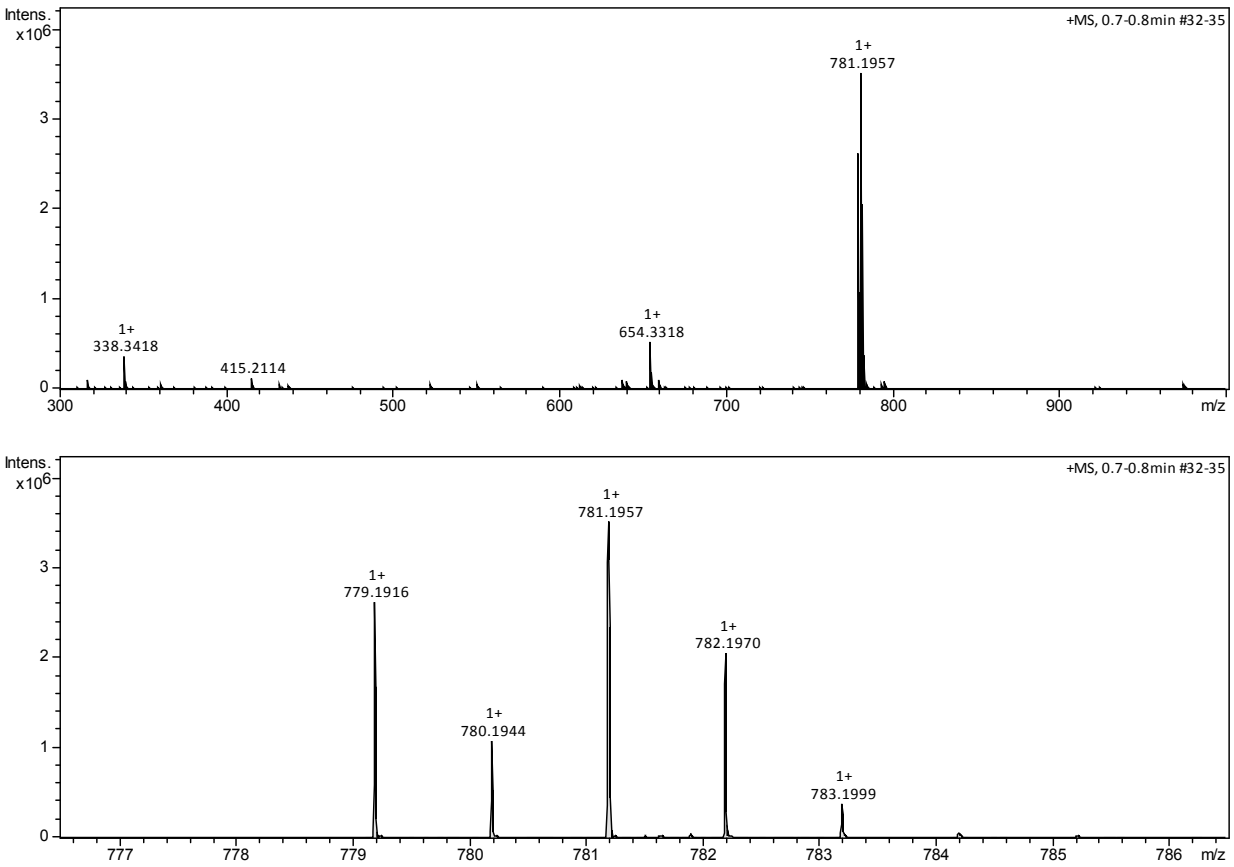

Figure SI3. Mass spectra for **pqiIrPhen** in acetonitrile.

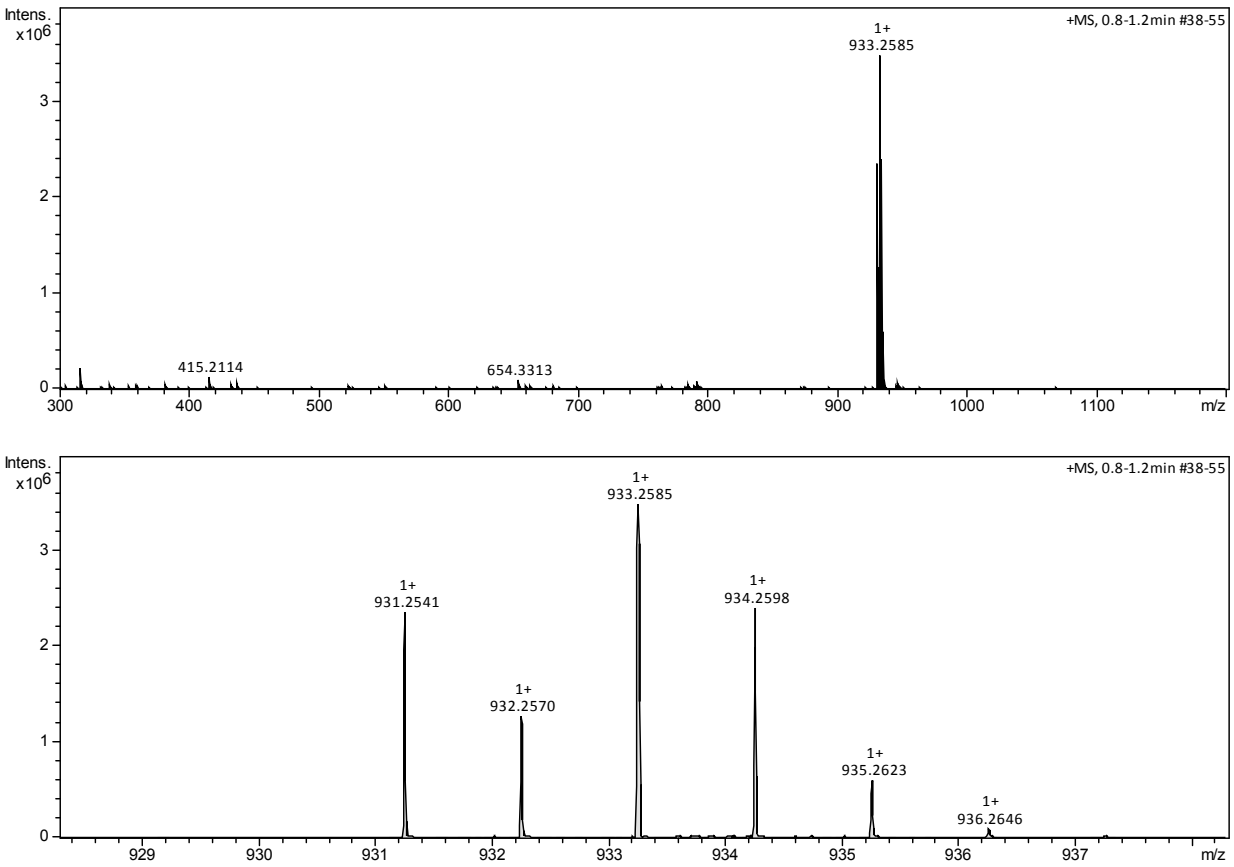

Figure SI4. Mass spectra for **pqiIrPh$_2$phen** in acetonitrile.

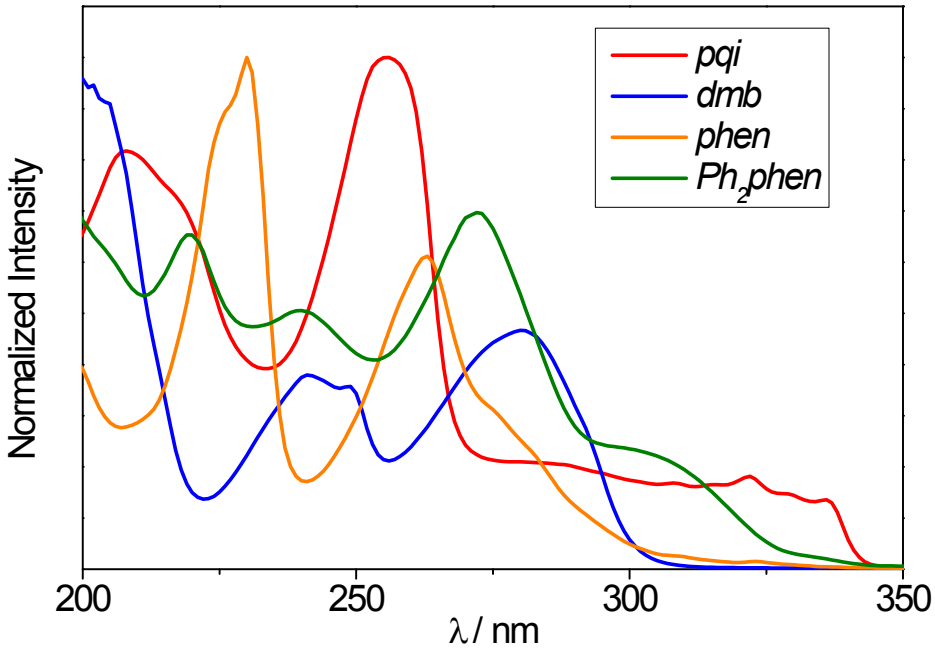

Figure SI5. Absorption spectra for the free, non-coordinated ligand in acetonitrile at 298 K. Tthe low energy ππ* transitions within the *pqi* ligands are more stabilized than for the *NN* ligands, hence $^{1}LC_{pqi}$ transitions exert a higher influence on the complex's light absorption at lower energies.

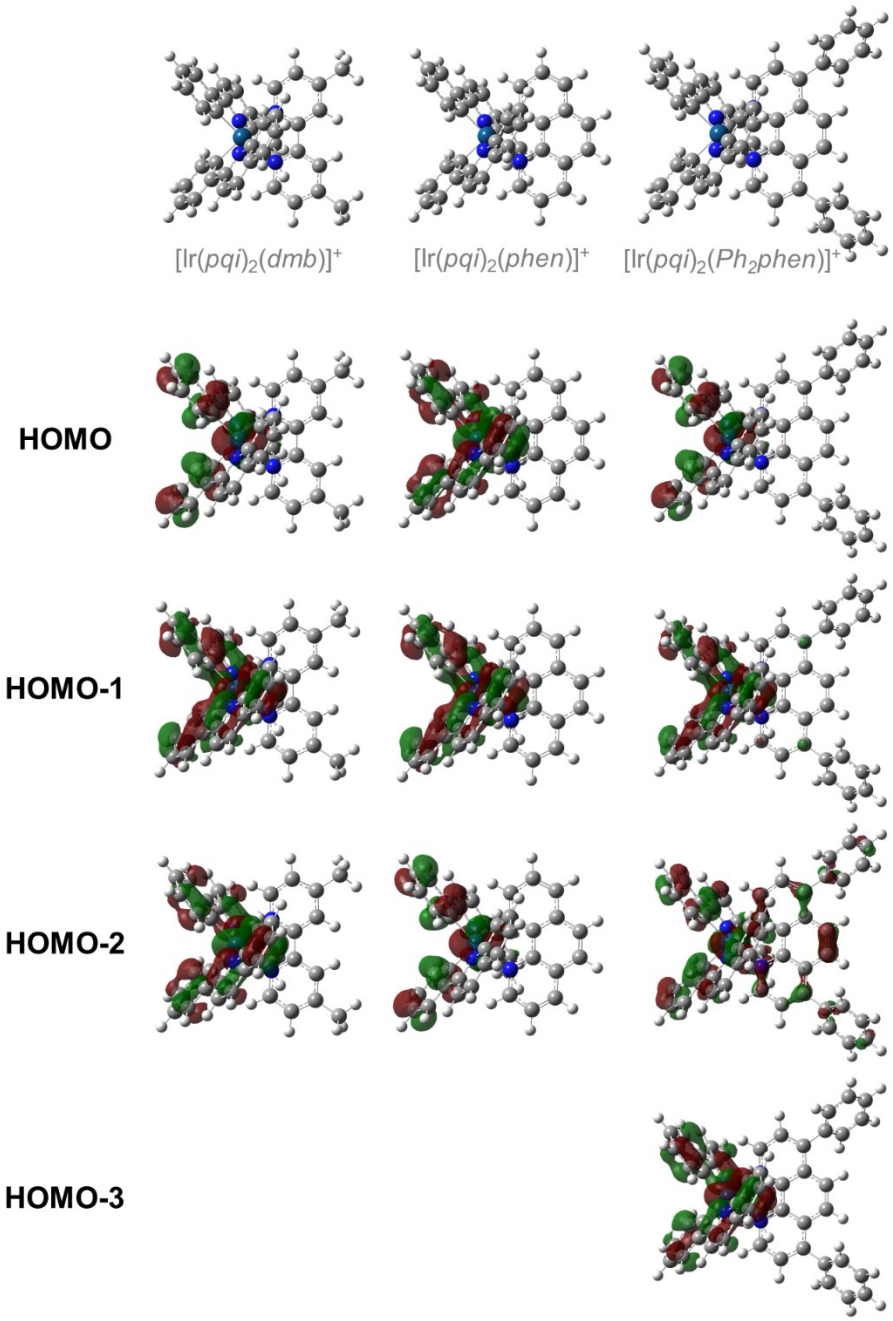

Figure SI6. Orbital contours (0.03 eÅ^{-3}) for HOMO sets related to S_1–S_4 and T_1–T_3 excited states in the [Ir(*pqi*)$_2$(*NN*)]$^+$ series.

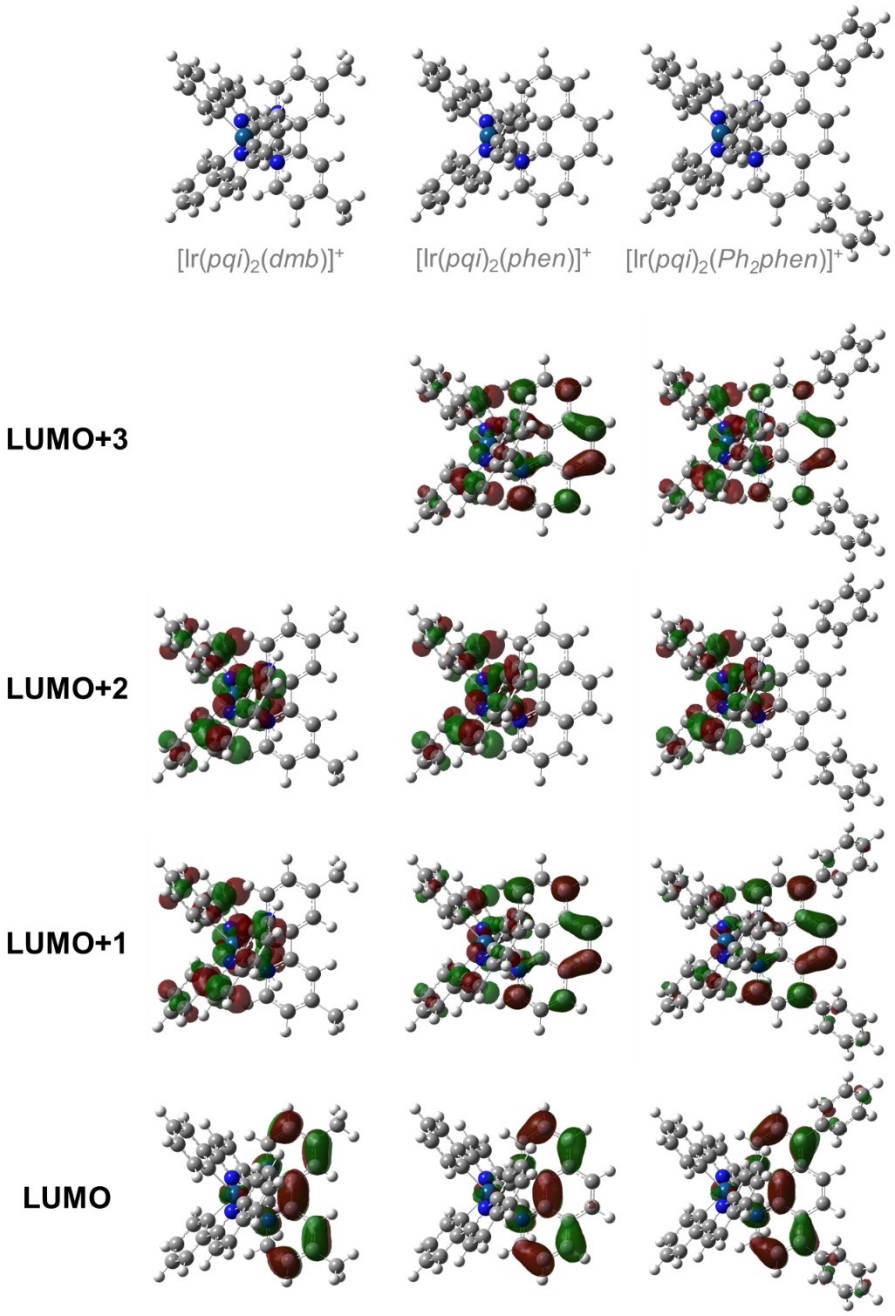

Figure SI7. Orbital contours (0.03 eÅ^{-3}) for LUMO sets related to S_1–S_4 and T_1–T_3 excited states in the [Ir(*pqi*)$_2$(*NN*)]$^+$ series.

Table SI1. Calculated Excited States for $[Ir(pqi)_2(dmb)]^+$ in CH_3CN.

Excited State	Transition	Energy (Wavelength)	Oscillator Strength
S_1	MO164 → MO165 (77%) MO164 → MO167 (23%)	2.6539 eV (467.17 nm)	0.0092
S_2	MO164 → MO166	2.7224 eV (455.42 nm)	0.0024
S_3	MO164 → MO167	2.7297 eV (454.20 nm)	0.0525
S_4	MO161 → MO165 (17%) MO163 → MO165 (83%)	3.3231 eV (373.10 nm)	0.0337
S_5	MO161 → MO166 (25%) MO163 → MO166 (75%)	3.3558 eV (369.46 nm)	0.0290
S_6	MO161 → MO167 (22%) MO163 → MO167 (78%)	3.3982 eV (364.85 nm)	0.0161
S_7	MO162 → MO165 (81%) MO163 → MO166 (19%)	3.4397 eV (360.45 nm)	0.0085
S_8	MO162 → MO167 (84%) MO163 → MO166 (16%)	3.5498 eV (349.27 nm)	0.0525
S_9	MO162 → MO166 (61%) MO163 → MO165 (16%) MO163 → MO167 (23%)	3.5566 eV (348.61 nm)	0.0275
S_{10}	MO162 → MO167 (28%) MO163 → MO166 (12%) MO164 → MO168 (60%)	3.5894 eV (345.42 nm)	0.0268
S_{11}	--	3.6359 eV (341.00 nm)	0.0065
S_{12}	--	3.6560 eV (339.13 nm)	0.1952
S_{13}	--	3.6883 eV (336.16 nm)	0.0439
S_{14}	--	3.7794 eV (328.06 nm)	0.0069
S_{15}	--	3.8105 eV (325.38 nm)	0.0338

HOMO: MO164, LUMO: MO165

Table SI2. Calculated Excited States for $[Ir(pqi)_2(phen)]^+$ in CH_3CN.

Excited State	Transition	Energy (Wavelength)	Oscillator Strength
S_1	MO162 → MO163	2.6030 eV (476.31 nm)	0.0004
S_2	MO162 → MO164	2.6529 eV (467.35 nm)	0.0002
S_3	MO162 → MO165	2.7323 eV (453.77 nm)	0.0620
S_4	MO162 → MO164 (14%) MO162 → MO166 (86%)	2.9249 eV (423.89 nm)	0.0059
S_5	MO159 → MO163 (19%) MO161 → MO163 (81%)	3.2737 eV (378.73 nm)	0.0431
S_6	MO159 → MO164 (22%) MO161 → MO164 (78%)	3.3072 eV (374.90 nm)	0.0384
S_7	MO160 → MO163	3.3824 eV (366.56 nm)	0.0002
S_8	MO159 → MO165 (16%) MO160 → MO164 (35%) MO161 → MO165 (49%)	3.4132 eV (363.25 nm)	0.0049
S_9	MO159 → MO163 (43%) MO160 → MO164 (57%)	3.4991 eV (354.33 nm)	0.0288
S_{10}	MO155 → MO165 (10%) MO158 → MO165 (10%) MO159 → MO166 (15%) MO161 → MO164 (17%) MO161 → MO166 (48%)	3.5307 eV (351.16 nm)	0.0045
S_{11}	--	3.5603 eV (348.24 nm)	0.0040
S_{12}	--	3.5788 eV (346.45 nm)	0.1236
S_{13}	--	3.5881 eV (345.54 nm)	0.0673
S_{14}	--	3.6845 eV (336.50 nm)	0.0577
S_{15}	--	3.7094 eV (334.24 nm)	0.0056

HOMO: MO162, LUMO: MO163

Table SI3. Calculated Excited States for $[Ir(pqi)_2(Ph_2phen)]^+$ in CH_3CN.

Excited State	Transition	Energy (Wavelength)	Oscillator Strength
S_1	MO202 → MO203	2.5732 eV (481.83 nm)	0.0010
S_2	MO202 → MO204	2.6197 eV (473.29 nm)	0.0007
S_3	MO202 → MO205	2.7275 eV (454.57 nm)	0.0600
S_4	MO202 → MO204 (18%) MO202 → MO206 (82%)	2.8743 eV (431.36 nm)	0.0050
S_5	MO200 → MO203 (17%) MO201 → MO203 (83%)	3.2163 eV (385.49 nm)	0.1207
S_6	MO200 → MO204 (16%) MO201 → MO204 (84%)	3.2478 eV (381.75 nm)	0.0860
S_7	MO198 → MO203 (22%) MO199 → MO203 (78%)	3.3520 eV (369.88 nm)	0.0015
S_8	MO194 → MO205 (13%) MO200 → MO205 (18%) MO201 → MO205 (69%)	3.3797 eV (366.85 nm)	0.0045
S_9	MO200 → MO203	3.4349 eV (360.96 nm)	0.0549
S_{10}	MO199 → MO205 (15%) MO200 → MO206 (14%) MO201 → MO204 (17%) MO201 → MO206 (54%)	3.4658 eV (357.74 nm)	0.0080
S_{11}	--	3.4987 eV (354.37 nm)	0.0195
S_{12}	--	3.5031 eV (353.93 nm)	0.0876
S_{13}	--	3.5704 eV (347.26 nm)	0.0762
S_{14}	--	3.6502 eV (339.66 nm)	0.0551
S_{15}	--	3.6707 eV (337.76 nm)	0.0161

HOMO: MO202, LUMO: MO203

Table SI4. Molecular-Orbital contributions for $[Ir(pqi)_2(dmb)]^+$ in CH_3CN.

Molecular Orbital	Eigenvalue /hartree	MO Population / %				
		Ir	*pqi*		*dmb*	
			phenyl	quinoline	bpy	methyl
172 (LUMO+7)	−0.00933	12.59	35.31	38.53	13.46	0.11
171 (LUMO+6)	−0.03966	1.59	10.34	35.02	50.18	2.87
170 (LUMO+5)	−0.04262	2.41	15.91	53.24	27.94	0.50
169 (LUMO+4)	−0.04321	0.27	6.66	46.82	44.55	1.70
168 (LUMO+3)	−0.05165	3.65	6.48	21.81	66.86	1.20
167 (LUMO+2)	−0.08052	3.02	15.02	78.37	3.46	0.13
166 (LUMO+1)	−0.08171	3.75	15.78	77.04	3.36	0.07
165 (LUMO)	−0.08372	3.39	0.64	3.82	87.99	4.16
164 (HOMO)	−0.20639	47.78	39.63	9.43	3.12	0.04
163 (HOMO−1)	−0.22873	30.63	27.18	37.96	4.01	0.22
162 (HOMO−2)	−0.23564	41.16	18.27	38.81	1.73	0.03
161 (HOMO−3)	−0.23830	32.98	33.18	28.88	4.63	0.33
160 (HOMO−4)	−0.24283	20.44	41.38	36.73	1.38	0.07
159 (HOMO−5)	−0.24677	5.35	78.14	11.85	4.60	0.06
158 (HOMO−6)	−0.25587	34.20	5.40	47.34	12.63	0.43
157 (HOMO−7)	−0.25600	29.11	5.53	54.88	10.04	0.44

Table SI5. Molecular-Orbital contributions for $[Ir(pqi)_2(phen)]^+$ in CH_3CN.

Molecular Orbital	Eigenvalue /hartree	MO Population / %				
		Ir	*pqi*		*phen*	
			phenyl	quinoline	phen	
170 (LUMO+7)	−0.01016	4.14	5.52	20.52	69.82	
169 (LUMO+6)	−0.03532	3.28	3.25	12.49	80.98	
168 (LUMO+5)	−0.04182	1.39	17.41	79.81	1.39	
167 (LUMO+4)	−0.04686	1.71	19.59	65.53	13.17	
166 (LUMO+3)	−0.07734	1.82	7.24	42.03	48.91	
165 (LUMO+2)	−0.08089	3.76	15.02	78.66	2.56	
164 (LUMO+1)	−0.08618	2.13	8.64	38.62	50.61	
163 (LUMO)	−0.08686	3.65	0.63	3.41	92.31	
162 (HOMO)	−0.20728	47.20	40.02	9.69	3.09	
161 (HOMO−1)	−0.22983	27.79	28.62	39.36	4.23	
160 (HOMO−2)	−0.23661	38.33	19.65	40.26	1.76	
159 (HOMO−3)	−0.23859	34.07	29.35	26.95	9.63	
158 (HOMO−4)	−0.24348	20.49	39.86	38.50	1.15	
157 (HOMO−5)	−0.24738	5.13	77.26	9.85	7.76	
156 (HOMO−6)	−0.25260	6.82	4.09	48.85	40.24	
155 (HOMO−7)	−0.25724	43.77	5.60	40.01	10.62	

Table SI6. Molecular-Orbital contributions for $[Ir(pqi)_2(Ph_2phen)]^+$ in CH_3CN.

Molecular Orbital	Eigenvalue /hartree	MO Population / %				
		Ir	*pqi*		*Ph₂phen*	
			phenyl	quinoline	phen	phenyl
210 (LUMO+7)	−0.02894	0.20	0.81	3.70	47.79	47.50
209 (LUMO+6)	−0.03901	1.80	5.40	18.48	60.07	14.25
208 (LUMO+5)	−0.04177	1.35	16.93	78.92	1.97	0.83
207 (LUMO+4)	−0.04730	1.68	16.66	56.52	21.99	3.15
206 (LUMO+3)	−0.07862	2.55	10.16	55.86	27.60	3.83
205 (LUMO+2)	−0.08070	3.66	15.08	78.97	2.27	0.02
204 (LUMO+1)	−0.08791	1.37	5.48	23.58	61.69	7.88
203 (LUMO)	−0.08824	3.73	0.49	2.68	83.60	9.50
202 (HOMO)	−0.20689	47.29	39.80	9.55	3.27	0.09
201 (HOMO−1)	−0.22878	33.84	22.03	32.61	8.87	2.65
200 (HOMO−2)	−0.23559	19.10	28.51	21.77	21.50	9.12
199 (HOMO−3)	−0.23626	39.18	19.25	39.27	2.08	0.22
198 (HOMO−4)	−0.24301	21.42	39.74	35.59	2.05	1.20
197 (HOMO−5)	−0.24502	2.41	44.02	20.18	23.73	9.66
196 (HOMO−6)	−0.24820	3.92	44.49	34.47	12.45	4.67
195 (HOMO−7)	−0.25357	19.57	3.84	29.95	20.32	26.32

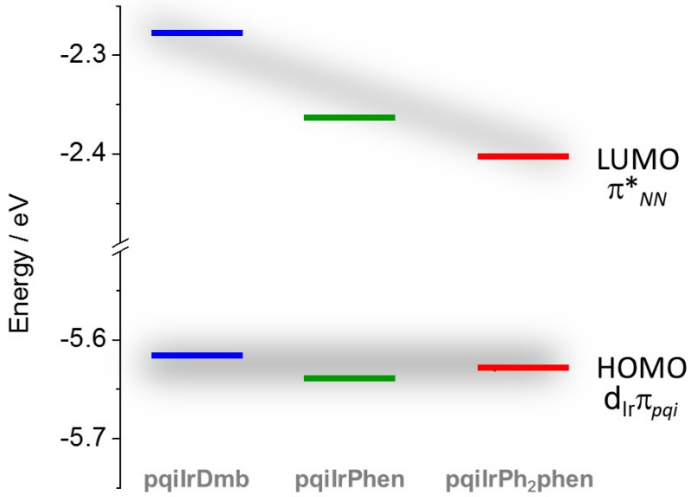

Figure SI8. HOMO and LUMO energies (involved in the S_1 transition) calculated by B3LYP/LanL2DZ (Ir) and B3LYP/6-31(d,p) (CHN). A typical trend for heteroleptic $[Ir(NC)_2(NN)]^+$ complexes[18–22] can be observed: the electron-donating CH_3 moiety in *dmb* increases the π^*_{NN} (LUMO) energy in opposite to electron-withdrawing phenyl groups in Ph_2phen that stabilizes π^*_{NN}; in parallel, the $d_{Ir}\pi_{pqi}$ (HOMO) energies are practically constant among the series since the three complexes have the same *pqi* cyclometalated ligand. Consequently, the S_1 state (HOMO → LUMO) in **pqiIrDmb** lies at a higher energy (2.654 eV; 467 nm) while **pqiIrPh2phen**'s S_1 is situated at a lower energy (2.573 eV; 482 nm). Such trend, however, cannot be directly observed in their experimental absorption spectra since the magnitude of the oscillator strength for S_3 transitions (HOMO → LUMO+2) at 454 nm is much higher than for S_1, overlapping the absorption contributions from S_1 and S_2 around 455 to 485 nm.

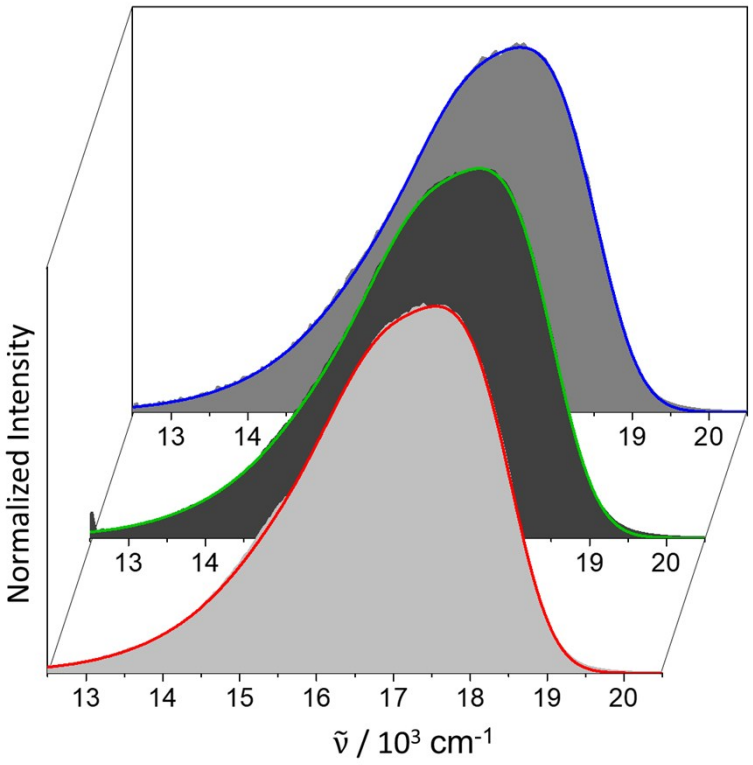

Figure SI9. Experimental (solid grey areas) and fitted emission spectra by use of Equation 1 of the Article with the parameters listed in Table 4 of the Article (colored solid curves) for the emission of **pqiIrDmb** (blue), **pqiIrPhen** (green) and **pqiIrPh$_2$phen** (red) in degassed acetonitrile at 298 K.

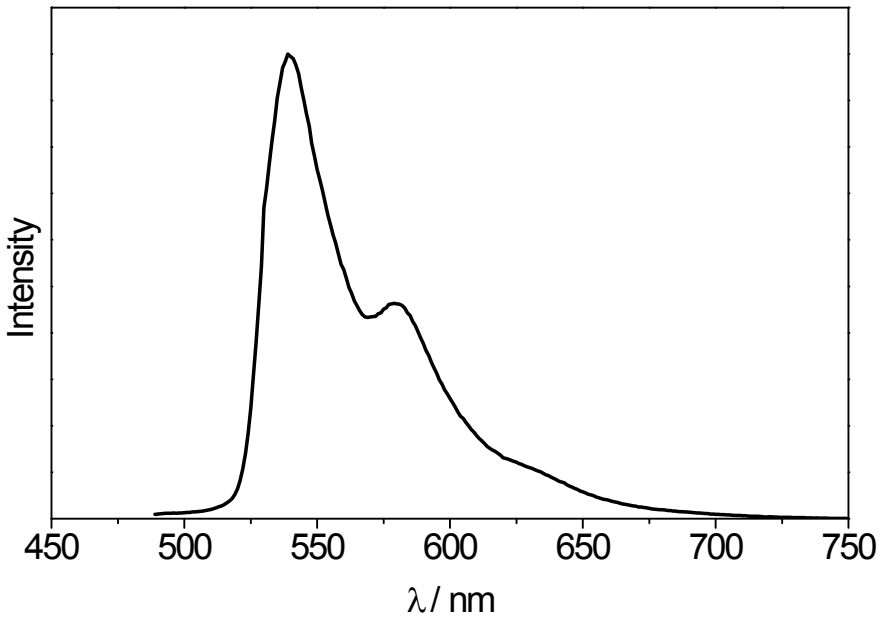

Figure SI10. Emission spectra for the free *pqi* ligand in prop:but at 77 K (λ_{em} = 360 nm), ascribed to the weak $^3\pi\pi^*$ phosphorescence.

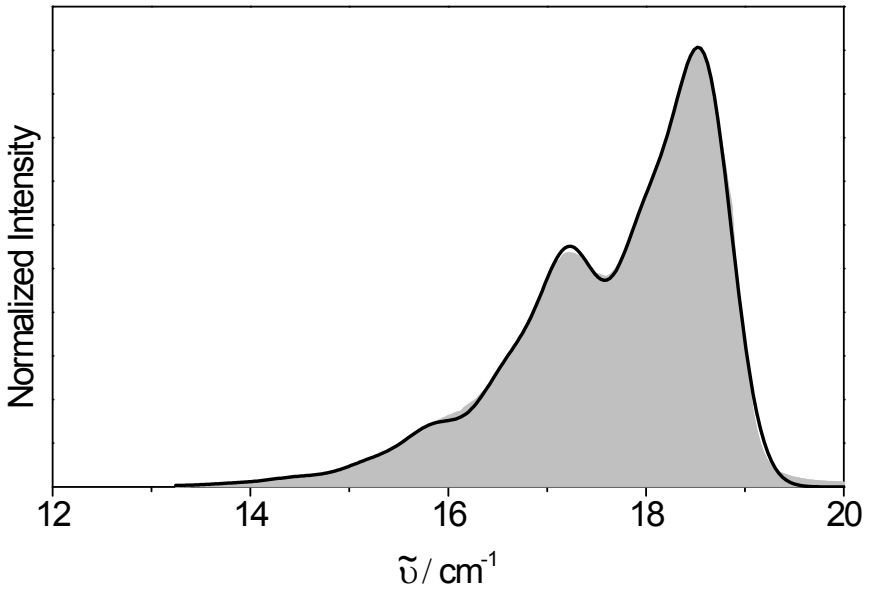

Figure SI11. Experimental (grey area) and simulated emission spectra by use of Equation 1 of the Article with the parameters listed in Table 4 of the Article (black solid curves) for the emission of the free *pqi* ligand in prop:but at 77 K.

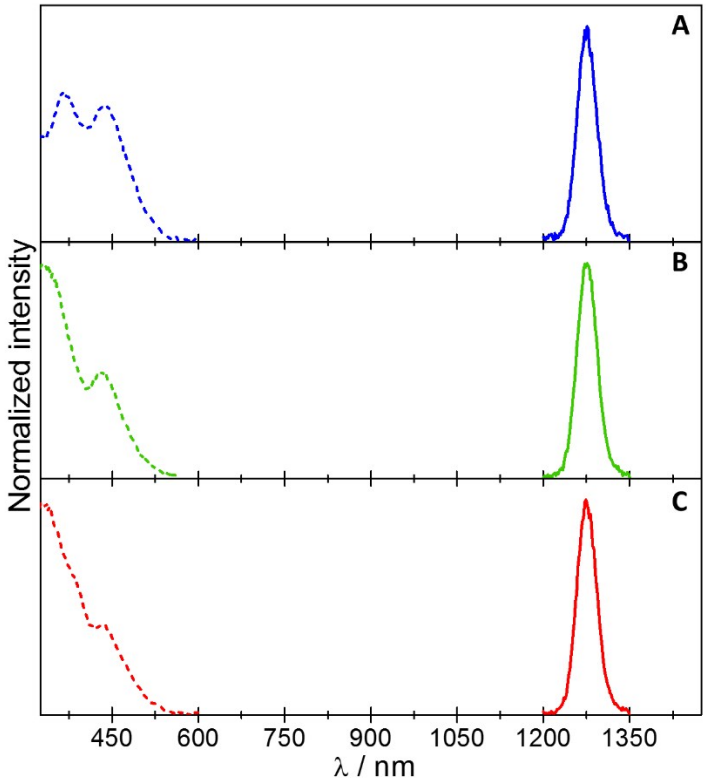

Figure SI12. Excitation (– – –, λ_{em} = 1270 nm) and emission spectra (——, λ_{exc} = 435 nm) of oxygen-saturated acetonitrile solutions of complexes **pqiIrDmb** (A, blue), **pqiIrPhen** (B, green) and **pqiIrPh$_2$phen** (C, red) at 298 K. For these solutions, the excitation spectra of the singlet oxygen's 1270 nm emission perfectly superimpose with the excitation spectra of the complex's 564 nm emission in degassed acetonitrile, including the direct excitation of the T_1 state around 525 nm. These facts indicate an efficient energy transfer from the complex to the oxygen, as ascertained by a favorable, spontaneous free energy change (ΔG_{en}^0) for energy transfer from complex's T_1 to oxygen's $^1\Delta_g$ (i.e. $\Delta G_{en}^0 = \Delta G_{1\Delta g} - \Delta G_{T1}$) that ranges from -10820 to -10880 cm^{-1} (considering $\Delta G_{1\Delta g}$ = 7940 cm^{-1} [23]), Table 6 in the Article.

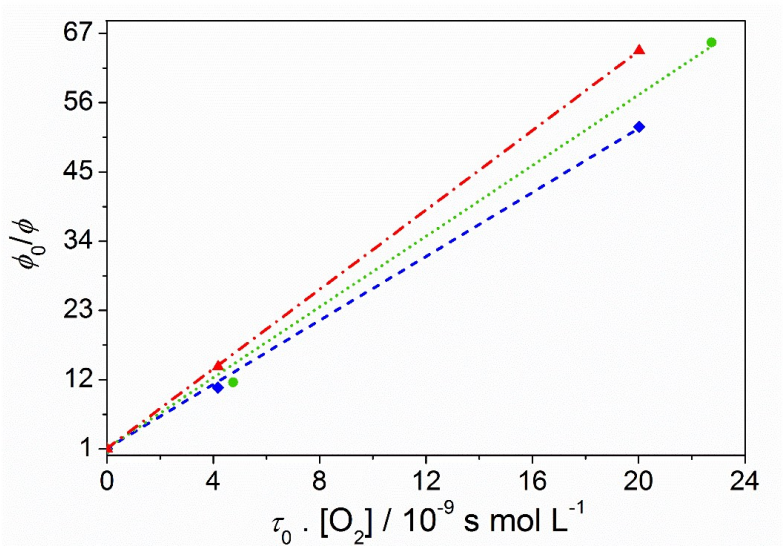

Figure SI13. Stern–Volmer plots for **pqiIrDmb** (♦, – – –, $R^2 = 0.9996$), **pqiIrPhen** (●, •••••, $R^2 = 0.9973$) and **pqiIrPh$_2$phen** (▲, –•–•, $R^2 = 0.9999$) in acetonitrile at 298 K.

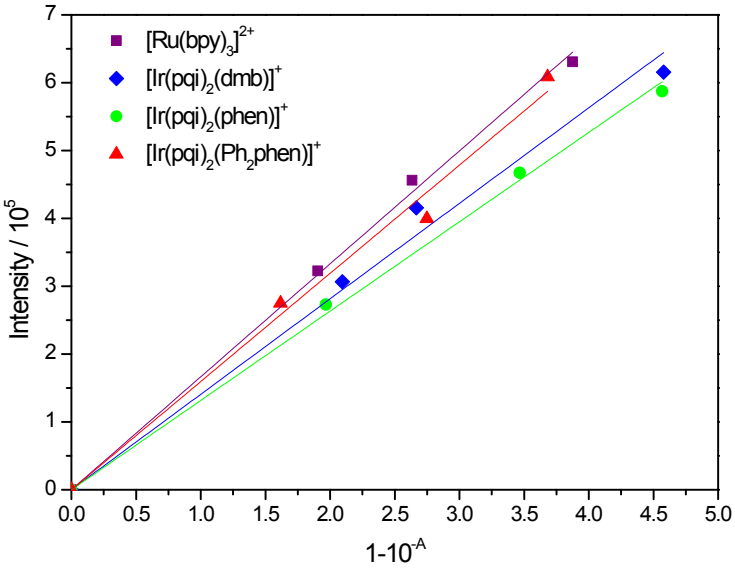

Figure SI14. Linear fits for the plots of 1-$10^{-A435nm}$ as a function of O_2's emission intensity around 1270 nm.

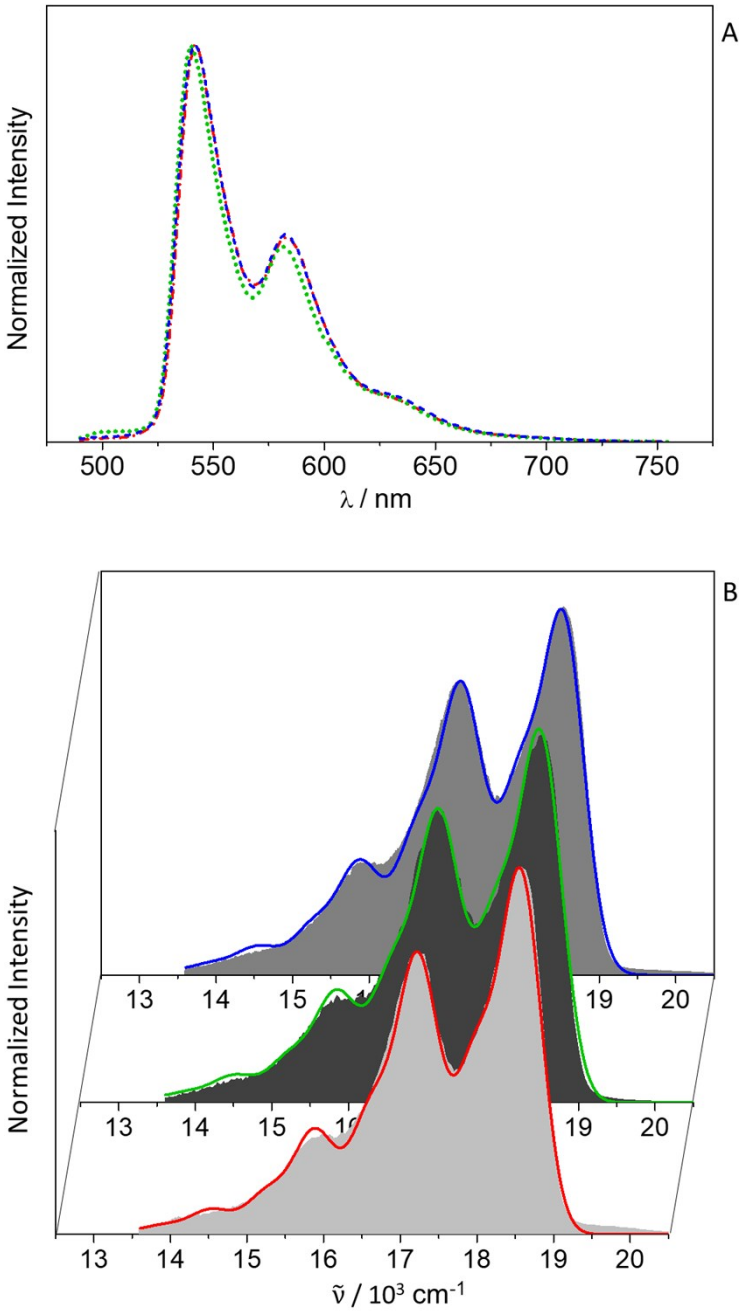

Figure SI15. Emission spectra for **pqiIrDmb** (blue – – –), **pqiIrPhen** (green •••) and **pqiIrPh$_2$phen** (red –•–•) in prop:but at 77 K: (A) Experimental spectra in wavelengths, with their CIE color coordinates shown in the inset; (B) Fitted emission spectra by use of Equation 1 of the Article with the parameters listed in Table SI7 (colored solid curves) overlapped to the experimental spectra in wavenumbers (solid grey areas).

Table SI7. Spectral fitting parameters for the emission of **pqiIrDmb**, **pqiIrPhen**, **pqiIrPh$_2$phen** and *pqi* at 77 K (in prop:but).

Compound	E_0 / cm^{-1}	$\tilde{\nu}_{1/2}$ / cm^{-1}	$\hbar\omega_H$ / cm^{-1}	S_H	$\hbar\omega_L$ / cm^{-1}	S_L	R
77 K prop:but							
pqiIrDmb	18540	620	1350	0.94	570	0.60	0.99823
pqiIrPhen	18520	640	1360	0.93	590	0.56	0.99847
pqiIrPh$_2$phen	18580	620	1370	0.92	590	0.55	0.99828
Free *pqi*H	18580	690	1400	0.56	600	0.63	0.99935

References

1 J. C. de Mello, H. F. Wittmann and R. H. Friend, *Adv. Mater.*, 1997, **9**, 230–232.

2 M. Grüner, V. Siozios, B. Hagenhoff, D. Breitenstein and C. A. Strassert, *Photochem. Photobiol.*, 2013, **89**, 1406–1412.

3 Á. Barroso, M. Grüner, T. Forbes, C. Denz and C. A. Strassert, *ACS Appl. Mater. Interfaces*, 2016, **8**, 15046–15057.

4 A. A. Abdel-Shafi, D. R. Worrall and A. Y. Ershov, *Dalt. Trans.*, 2004, 30–36.

5 A. Ito, D. J. Stewart, T. E. Knight, Z. Fang, M. K. Brennaman and T. J. Meyer, *J. Phys. Chem. B*, 2013, **117**, 3428–3438.

6 CIE-Datatables, *http://www.cie.co.at/publ/abst/datatables15_2004/z2.txt; http://www.cie.co.at/publ/abst/datatables15_2004/x2.txt; http://www.cie.co.at/publ/abst/datatables15_2004/y2.txt*, .

7 D. Fylstra, L. Lasdon, J. Watson and A. Waren, *Interfaces (Providence).*, 1998, **28**, 29–55.

8 C. A. Parker and W. T. Rees, *Analyst*, 1960, **85**, 587–600.

9 M. J. Frisch, G. W. Trucks, H. B. Schlegel, G. E. Scuseria, M. A. Robb, J. R. Cheeseman, G. Scalmani, V. Barone, B. Mennucci, G. A. Petersson, H. Nakatsuji, M. Caricato, X. Li, H. P. Hratchian, A. F. Izmaylov, J. Bloino, G. Zheng, J. L. Sonnenberg, M. Hada, M. Ehara, K. Toyota, R. Fukuda, J. Hasegawa, M. Ishida, T. Nakajima, Y. Honda, O. Kitao, H. Nakai, T. Vreven, J. A. M. Jr., J. E. Peralta, F. Ogliaro, M. Bearpark, J. J. Heyd, E. Brothers, K. N. Kudin, V. N. Staroverov, R. Kobayashi, J. Normand, K. Raghavachari, A. Rendell, J. C. Burant, S. S. Iyengar, J. Tomasi, M. Cossi, N. Rega, N. J. Millam, M. Klene, J. E. Knox, J. B. Cross, V. Bakken, C. Adamo, J. Jaramillo, R. Gomperts, R. E. Stratmann, O. Yazyev, A. J. Austin, R. Cammi, C. Pomelli, J. W. Ochterski, R. L. Martin,

K.Morokuma, V. G. Zakrzewski, G. A. Voth, P. Salvador, J. J. Da, O. Farkas, J. B. Foresman, J. V. Ortiz, J. Cioslowski and D. J. Fox, *Gaussian 09, Revis. A.1, Gaussian, Inc., Wallingford CT*.

10 P. J. Hay and W. R. Wadt, *J. Chem. Phys.*, 1985, **82**, 270–283.

11 W. R. Wadt and P. J. Hay, *J. Chem. Phys.*, 1985, **82**, 284–298.

12 P. J. Hay and W. R. Wadt, *J. Chem. Phys.*, 1985, **82**, 299–310.

13 C. Lee, W. Yang and R. G. Parr, *Phys. Rev. B*, 1988, **37**, 785–789.

14 A. D. Becke, *J. Chem. Phys.*, 1993, **98**, 5648–5652.

15 J. Tomasi, B. Mennucci and R. Cammi, *Chem. Rev.*, 2005, **105**, 2999–3094.

16 G. Scalmani and M. J. Frisch, *J. Chem. Phys.*, 2010, **132**, 114110.

17 R. Dennington, T. Keith and J. Millam, *GaussView, Version 5, Semichem Inc Shawnee Mission KS*.

18 C.-J. Chang, C.-H. Yang, K. Chen, Y. Chi, C.-F. Shu, M.-L. Ho, Y.-S. Yeh and P.-T. Chou, *Dalt. Trans.*, 2007, **2007**, 1881–1890.

19 H. Li, P. Winget, C. Risko, J. S. Sears and J.-L. Brédas, *Phys. Chem. Chem. Phys.*, 2013, **15**, 6293–62302.

20 T. Tsuboi and W. Huang, *Isr. J. Chem.*, 2014, **54**, 885–896.

21 K. P. S. Zanoni, R. L. Coppo, R. C. Amaral and N. Y. Murakami Iha, *Dalt. Trans.*, 2015, **44**, 14559–14573.

22 M. S. Lowry and S. Bernhard, *Chem. Eur. J.*, 2006, **12**, 7970–7977.

23 M. C. DeRosa and R. J. Crutchley, *Coord. Chem. Rev.*, 2002, **233–234**, 351–371.